PHOTONICS Research

Hybrid silicon nonlinear photonics [Invited]

Ming Li,[1] Lin Zhang,[2] Li-Min Tong,[1] and Dao-Xin Dai[1,*]

[1]Centre for Optical and Electromagnetic Research, JORCEP, State Key Laboratory for Modern Optical Instrumentation, Zhejiang Provincial Key Laboratory for Sensing Technologies, Zhejiang University, Hangzhou 310058, China
[2]Key Laboratory of the Ministry of Education on Optoelectronic Information Technology, School of Precision Instruments and Optoelectronics Engineering, Tianjin University, Tianjin 300072, China
*Corresponding author: dxdai@zju.edu.cn

Received 15 November 2017; revised 18 January 2018; accepted 18 January 2018; posted 19 January 2018 (Doc. ID 312497); published 11 April 2018

Nonlinear silicon photonics has shown an ability to generate, manipulate, and detect optical signals on an ultra-compact chip at a potential low cost. There are still barriers hindering its development due to essential material limitations. In this review, hybrid structures with some specific materials developed for nonlinear silicon photonics are discussed. The combination of silicon and the nonlinear materials takes advantage of both materials, which shows great potential to improve the performance and expand the applications for nonlinear silicon photonics. © 2018 Chinese Laser Press

OCIS codes: (190.4390) Nonlinear optics, integrated optics; (230.4320) Nonlinear optical devices; (130.3130) Integrated optics materials.

https://doi.org/10.1364/PRJ.6.000B13

1. INTRODUCTION

Silicon nonlinear photonics has been developed to meet the demand of on-chip optical processing and computation, owing to its potential low cost and CMOS compatibility [1–3]. The ability of strong optical confinement and a large third-order nonlinear susceptibility has greatly encouraged research in this area in the past two decades. An on-chip optical information processor requires the monolithic integration of light sources, optical switches, optical modulators, and photodetectors [4]. High-speed optical signal processing [5–7], signal detection, optical sensing [8], optical modulation [9], and broadband wavelength conversion [10] have already become achievable on a silicon chip. Parametric amplification, Raman lasing, and Brillouin lasing provide the route for on-chip photon generation [11–15].

However, the development of nonlinear photonics on silicon is still limited by the essential shortcomings of silicon. As a centrosymmetric material, silicon does not have the second-order nonlinear susceptibility, which is essential for efficient electro-optic modulation and second harmonic generation. The optical parametric nonlinear process observed commonly in silicon is the third-order process, including self-phase modulation, cross-phase modulation, and four-wave mixing [16–19]. Generally, the $\chi^{(3)}$ susceptibility is several orders of magnitude lower than the $\chi^{(2)}$ susceptibility. Even though a slow light effect in a photonic crystal waveguide can be used to enhance the nonlinear interaction [20,21], the third-order nonlinear process is not efficient compared to the second-order process.

What's more, the band gap of silicon is 1.1 eV, which is smaller than the energy of two photons at the wavelength around 1550 nm, so silicon suffers from two-photon absorption (TPA) in the near-infrared. The absorption rate depends on the intensity of the incident field, which limits its application in situations requiring a large pump power (i.e., parametric amplification, Raman lasing, and Brillouin amplification) [12,13,22–24]. As a consequence of TPA, the absorption of photons may generate free carriers [25]. The optical property of silicon depends on both the bounded electrons and the free carriers. The dielectric constant is described by the sum of the Lorentz model and the Drude model. The density of the free carriers can not only modify the real part of the dielectric constant, but also add an imaginary part. The plasma effect supported by the free carriers leads to the absorption of photons, which results in detrimental energy waste and unwanted heat. In addition, the lifetime of free carriers ranges from a picosecond to a nanosecond, which limits the speed of the modulators. The nonlinear absorptions from TPA and free carrier absorption (FCA) are two obstacles in nonlinear silicon photonics. Even though FCA can be mitigated by removing the generated free carriers in silicon by integrating the devices within the p–i–n diode, the modified silicon material is still inferior to polymer and silicon nitride, and it is hard to meet the demand of high performance nonlinear photonic devices.

To overcome these drawbacks and improve the performance of devices on the silicon platform, various materials with a better nonlinear property are introduced [7–9,13]. These materials

are integrated with silicon using some smart structures to form a hybrid platform, which takes advantage of both materials simultaneously. These silicon hybrid platforms not only can overcome the shortcomings of silicon, but also can enrich the function of silicon photonics and improve the flexibility.

Two kinds of hybrid structures with distinct designs have been developed. The first one can be summarized as modifying the internal structure of silicon itself to obtain the desired nonlinearity. The other method introduces new materials with better nonlinear property to integrate with silicon. These new materials provide the desired nonlinearity while silicon confines the optical modes to nanoscale.

Here, we review the recent progress in hybrid silicon nonlinear photonics. First, we introduce the hybrid structures used to modify the nonlinear property of silicon. Two kinds of structures are discussed to break the essential symmetry and add the second-order nonlinear susceptibility on silicon. The free carrier density can also be controlled using p–i–n junctions. Next, we review the commonly used hybrid structures with new materials for enhancing the nonlinear photonic effects, including bulk materials and layered materials. Finally, we give a short summary.

2. MODIFICATION OF SILICON FOR NONLINEAR PHOTONICS

In this section, we focus on the first kind of hybrid structure, in which the structures can change the nonlinear optical property of silicon. The materials introduced only work as auxiliaries and do not contribute directly to the nonlinear process by themselves.

A. Enhancement of $\chi^{(2)}$ Nonlinearity in Silicon

Because $\chi^{(2)}$ nonlinearity strongly depends on the inversion symmetry of materials, it is possible to induce $\chi^{(2)}$ nonlinearity in silicon by breaking the inversion symmetry of the crystal lattice. Here we discuss two methods to break the symmetry.

Straining layers of Si_3N_4 deposited on top of silicon waveguides can provide stress gradient to break the symmetry of the crystal lattice [26,27]. Figures 1(a) and 1(b) show a silicon photonic crystal waveguide strained by Si_3N_4 layers. The inhomogeneous change of the silicon lattice was verified by Raman spectroscopy. Consequently, the strained silicon exhibits strong $\chi^{(2)}$ nonlinearity up to 40 pm/V, which provides a method for electro-optic modulation, second harmonic generation, and sum frequency generation on silicon [28]. In Ref. [28], the authors experimentally demonstrated the second harmonic generation efficiency of 0.01%/W in a 2 mm long strained silicon waveguide. Periodically strained silicon can be used to achieve quasi-phase matching [29], thus realizing higher conversion efficiency. An alternative approach to increase the $\chi^{(2)}$ nonlinear interaction is the photonic crystal waveguide geometry. It has been demonstrated that the photonic crystal waveguide structure is compatible with the strained silicon structure, in which the group velocity of light can be slowed down to 1/100 of the vacuum light speed. In addition, resonant configurations also show great potential to enhance the nonlinear interaction.

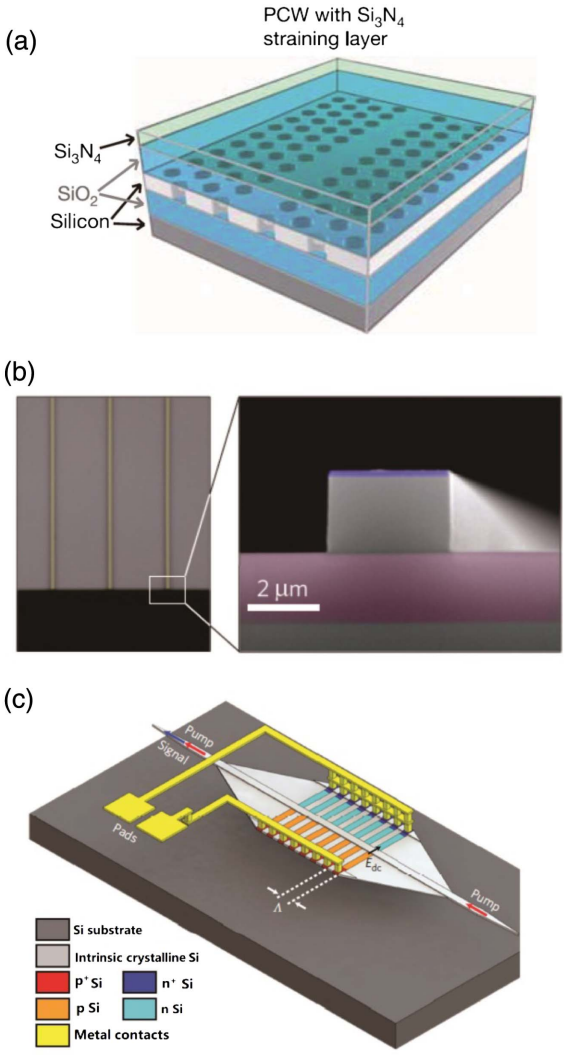

Fig. 1. (a) Diagram of the investigated silicon photonic crystal waveguide with Si_3N_4 straining layers on top [26]. (b) A top-view optical image of the strained silicon waveguides where a few waveguides are observed as yellow lines. A scanning electron microscopy image of the input facet of the waveguide is also shown. The waveguide is designed to realize second harmonic generation from mid-infrared to near-infrared [28]. (c) Three-dimensional sketch of the electric-field-induced second harmonic generation device with silicon ridge waveguide and spatially periodic patterning of the p–i–n junction. The electric field across the p–i–n junction induces the second-order nonlinear effect in a silicon waveguide. The periodic pattern is designed to alter the nonlinear susceptibility periodically for quasi-phase matching [30].

In addition to the mechanical method, the $\chi^{(3)}$ nonlinearity of silicon offers another way to induce $\chi^{(2)}$ nonlinearity. By applying an electric field across the silicon, the dipoles moments orient parallel to the electric vectors and the symmetry is broken. The induced $\chi^{(2)}$ nonlinearity can also be treated as DC electric field amplified $\chi^{(3)}$ nonlinearity. The $\chi^{(3)}$ nonlinearity enables the four-wave mixing of the optical field and the static electric field. In the presence of one non-oscillating electric field E_0 and two fields with frequency $\omega_{1,2}$, the nonlinear term of the polarizability is $P_{\mathrm{nl}} \approx \chi^{(3)} E_0 E_1 E_2$, where E_i represents the oscillating field with frequency ω_i.

The third-order nonlinear interaction can be effectively treated as the second-order interaction between E_1 and E_2 with effective $\chi^{(2)} \approx \chi^{(3)} E_0$. The mixing of one optical field and three electric fields modulates the dielectric constant, which is known as the quadratic electro-optic effect. By fabricating compact p–i–n junction structures, the electric field is concentrated across the silicon waveguide. Since the breakdown field of silicon is as large as 4×10^7 V/m and the $\chi^{(3)}$ susceptibility is about the order of 10^{-18} m^2/V^2, the upper bound of the induced $\chi^{(2)}$ nonlinear susceptibility can be approximately calculated as 100 pm/V. In Ref. [30], an electric field induced $\chi^{(2)}$ susceptibility of 41 pm/V was achieved. In Fig. 1(c), the researchers can control each p–i–n junction individually to synthesize effective $\chi^{(2)}$ with a period of $1/\Delta k$ (Δk is the phase mismatch) along the waveguide, thus periodically "pooling" silicon and realizing quasi-phase matching. In this way, the efficiency of the second harmonic generation is promoted to 13% W^{-1} at 2.29 μm wavelength. Compared with 10^{-5} W^{-1} for an Si_3N_4 layer strained waveguide, in which phase matching is quite difficult, this method shows high flexibility in modifying the second-order nonlinearity of silicon.

Even though these two methods can induce $\chi^{(2)}$ nonlinearity in silicon, TPA and FCA still remain as the main obstacles when the pump is high. In the scheme using p–i–n junction, the free carriers' density will more or less be influenced, which alters the nonlinear response of silicon in other aspects. The voltage should also be carefully controlled to avoid the breakdown of the silicon.

B. Manipulation of Free-Carriers in Silicon

Generally, the parametric nonlinear process requires a very high pump, while the essential and TPA-generated carriers induce parasitic nonlinear loss. In the resonant configuration, the threshold of the parametric oscillator and the Raman laser is proportional to the optical loss. The absorption of the free carriers pushes the pump threshold to values difficult to reach. Below the threshold, silicon is often used for quantum photon pair generation. The nonlinear loss significantly degrades the performance of the photon sources. Besides the loss effect, the lifetime of free carriers and the influence on the refractive index of silicon should also be considered.

An effective way to mitigate the influence of FCA is to control the density of free carriers in silicon. Fortunately, the reverse biased p–i–n diode can move the free carriers out of silicon. This method has been used to achieve net Raman gain in a silicon waveguide [31] and build low-threshold continuous wave Raman silicon laser [32]. For a silicon quantum photon source, increasing the coincidence-to-accidental and generation rates of quantum entangled photon pairs is also demonstrated in a silicon microcavity [33]. In addition, the reduction of the free carriers' density enables the high-speed wavelength conversion [5] via four-wave mixing.

Even though FCA plays a negative role due to the absorption of free carriers, one should be aware that the real part of the refractive index also depends on the free carriers' density. This provides an additional method to build modulators by modulating the density of the free carriers in silicon. High-speed electro-optic modulators up to 40 Gb/s have already been demonstrated on a silicon chip [34].

3. BULK-MATERIAL-ASSISTED SILICON NONLINEAR PHOTONICS

In the above section, we mainly focus on hybrid structures used to remold the essential properties of silicon. However, the hybrid structures require careful design and fabrication, and TPA and FCA still remain as the limitations. A more radical method is to introduce new materials to replace parts of the nonlinear function of silicon. By exploiting new materials with the desired nonlinear properties and making hybrid silicon photonic devices, the advantages of both materials can be used. Generally, there are three guidelines to select new materials: (1) the material should possess better nonlinear properties to compensate the shortcomings of silicon, such as second-order nonlinearity, larger third-order nonlinearity, and lower TPA rates; (2) the combination of the new material and silicon should not destroy the confinement property provided by silicon; and (3) the material should be CMOS-compatible. In the following section, we divide the materials into bulk materials and layered materials. These two types of materials for a silicon hybrid platform have different functions and require different structure designs, based on their shapes, integration methods, and optical properties.

Bulk materials are often used for the cladding of silicon waveguides. In this case, the materials not only contribute to the mode distributions, but also offer nonlinearities. It should be noted that the refractive index of most materials is lower than that of silicon, so the mode confinement offered by silicon may be destroyed while the nonlinear interaction strength scales as the inverse of the effective mode area $1/A_{\text{eff}}$ for waveguide mode. The most popular waveguide structures used to reduce the effective mode area and achieve stronger nonlinear interaction are nanoslot waveguides. A nanoslot waveguide consists of two silicon core regions with a low-index nanoslot between them. Due to the continuity of the perpendicular electric displacement vector at the silicon–slot interface, the electric field is greatly enhanced in the low-index nanoslot. The materials are filled in the slot and provide the required nonlinearity, while the mode confinement structure increases the nonlinear interaction. Another promising method is to harness the strong confinement of surface plasmons. Silicon hybrid plasmonic waveguides can be engineered to obtain ultrasmall modes. It has been theoretically demonstrated that high-speed optical modulation and four-wave mixing can be greatly enhanced in silicon devices with very small footprints [35,36]. However, the applications for devices of this type are hindered by the absorption of the plasmonic modes [37]. A low-loss silicon hybrid plasmonic waveguide may provide a solution [38]. In other configurations, the interaction between a resonant plasmonic structure and a single molecule in the strong coupling regime has been experimentally demonstrated [39], which may encourage the research of nonlinear photonics with silicon hybrid plasmonic structures.

Since the hybrid structures are complex and the refractive indexes of the new materials are different from that of silicon, the geometries should be carefully designed to simultaneously fulfill the phase-matching condition, the dispersion properties, and large mode overlap, as well as the tight mode confinement [40].

A. Utilization of Bulk Materials with Large $\chi^{(2)}$ Nonlinearity

Due to the symmetric property of the lattice, the second-order nonlinear susceptibility of bulk silicon is approximately zero. However, $\chi^{(2)}$ nonlinearity is necessary for electro-optic modulation, second harmonic generation, and sum frequency generation. Except for the methods described in Section 2, an obvious way to generate $\chi^{(2)}$ nonlinearity on silicon is to add a novel material with high $\chi^{(2)}$ onto silicon. This silicon hybrid platform can simultaneously benefit from the mode confinement from silicon and the $\chi^{(2)}$ nonlinearity from the new material. There are many materials that possess high second-order nonlinear coefficients. Some kinds of polymer and organic materials, such as DAST [41] and M1 [42], have $\chi^{(2)}$ susceptibility up to several hundred pm/V, which is much higher than most crystal materials, even the commonly used lithium niobate. It has been theoretically predicted that electro-optic polymer can be used as the cladding and filled in the nanoslot waveguides to build low voltage modulators toward millivolt [43]. A half-wave voltage of 0.25 V electro-optic modulator on silicon was recently experimentally demonstrated [44] using cladding polymer consisting of a highly active chromophore (YLD_124) doped 25% by weight into an inert host polymer [9]. It has also been demonstrated that organic materials with a $\chi^{(2)}$ coefficient high to several hundred pm/V can be compatibly integrated with silicon, which is promising for parametric down conversion, mid-infrared generation, and low-pump parametric amplification [45]. To fulfill the phase-matching condition of frequency conversion, the geometry of the nanoslot waveguides should be carefully engineered. The electro-optic polymers can also be combined with the photonic-crystal waveguide and resonant structures to enhance the electro-optic modulation efficiency and reduce the size of the device.

B. Utilization of Bulk Materials with Large $\chi^{(3)}$ Nonlinearity

In traditional nonlinear silicon photonics, third-order nonlinearity has been used to realize super-continuum generation, four-wave mixing, and photon pair generation. However, the competition between Kerr, and TPA and FCA effects has been a crucial topic for a long time. Even though silicon has a relative high $\chi^{(3)}$ susceptibility, the TPA effect becomes an issue when the pump power is relatively high, under which two photons can excite electron-hole pairs and generate free carriers. The nonlinear absorption rate scales quadratically with the intensity of the electric field, so the density of free carriers also increases rapidly with the pump power, which results in the absorption of photons and a change of both the real and imaginary parts of the dielectric constant of silicon. The TPA and FCA effects are highly destructive on nonlinear silicon photonics at the near-infrared region. It not only wastes energy and generates heat, but it also limits the performance of nonlinear devices, including low modulation speed, a high optical parametric threshold, and a low generation rate of the quantum photon source. A favorable platform providing strong nonlinear interaction requires a high Kerr-to-TPA ratio, which can be defined as a figure of merit (FOM) of nonlinear materials, as well as a Kerr nonlinear coefficient. The FOM is defined as

$$\mathrm{FOM} = \frac{\mathrm{Re}[n_2]}{4\pi\,\mathrm{Im}[n_2]}. \tag{1}$$

The complex number n_2 shows the linear relation between the refractive index n and the light intensity I, $n = n_0 + n_2 I$. It is possible to achieve a high FOM by choosing a long wavelength [46,47], where the energy of photon is small to excite the electron–hole pairs. An alternative to alleviate the influence of TPA is using nonlinear materials with a low TPA coefficient as the cladding for a silicon stripe waveguide or the internal materials in a silicon nanoslot waveguide [48,49]. The organic nonlinear materials [50–53] were introduced to build the silicon-organic hybrid structure [Fig. 2(a)]. Organic materials such as p-toluene sulphonate [54], DDMEBT [55], carotenoid [56], and azobenzene [57] have $\chi^{(3)}$ at the order of or even higher than 10^{-18} $\mathrm{m^2/V^2}$, while the TPA effect is not an issue in such materials [54]. In addition, the refractive index is under 2, which is well below silicon, making it suitable for the low-index material in the nanoslot waveguide. A silicon-organic hybrid waveguide has shown the ability to increase the FOM from 0.36 of silicon to 2. The low FCA effect allows high-speed, all-optical switching, modulation, and efficient wavelength conversion in waveguides [2,7,48,55,58]. Figure 2(b) shows all-optical demultiplexing of 170.8–42.7 Gb/s with a 4 mm long silicon-organic hybrid waveguide.

Similar to organic materials, silicon–chalcogenide (SC) is another promising hybrid silicon structure with a high FOM. It is well known that chalcogenide has a higher Kerr nonlinearity and a lower TPA rate than silicon [59]. With careful

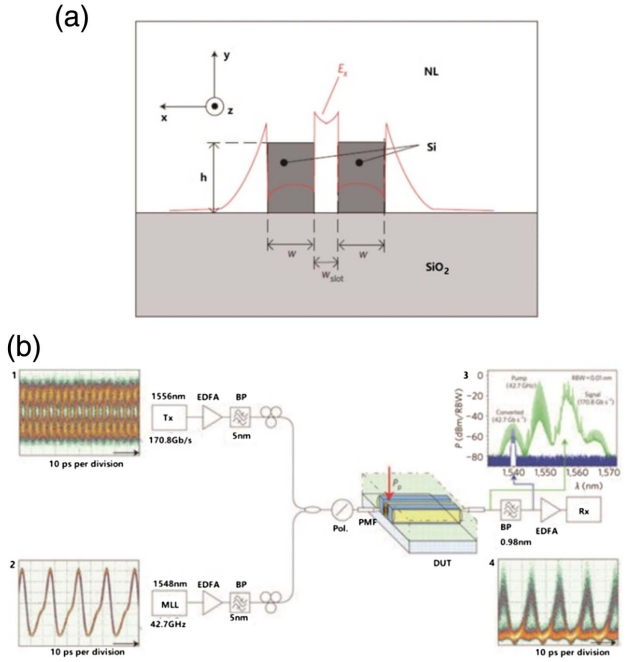

Fig. 2. (a) Schematic of a nanoslot waveguide covered by a nonlinear optical organic material. (b) Experimental setup of the all-optical demultiplexing by four-wave mixing. Inset: 1, diagram of the 170.8 Gb/s data signal; 2, diagram of the 42.7 GHz pump; 3, the spectrum at the output of the DUT (green) and after band-pass-filtering (blue); 4, diagram of the demultiplexed 42.7 Gb/s signal [7].

optimization for the structural design, the SC structure can significantly increase the FOM factor by five times [60]. Despite the organic and inorganic materials, nanocomposites can also be used to exploit new hybrid approaches (Si–Si nc) [61]. Si nanocrystal has Re[$\chi^{(3)}$] that are 2–3 orders of magnitude higher than silicon and is fully compatible with CMOS foundry. Silicon nanocrystal also has a refractive index close to silica, and thus is suitable to be used for nanoslot waveguides. It has been demonstrated by nonlinear measurements that the hybrid Si–Si nc structure shows low TPA and free carrier effect. The FOM of the slot waveguide structures can be increased to 2.9 [62]. Based on a Si–Si nc hybrid structure, it is efficient to realize third harmonic generation from mid-IR to near-IR [63], continuous-wave Raman amplification [64], ultrafast all-optical switching [65], and optical spectral quantization [66]. By engineering the dispersion of the hybrid silicon structures, it is also possible to realize broadband wavelength conversion and excite optical solitons [67,68]. Another benefit is that the TPA and FCA effects in silicon are relatively low because most energy is confined in the nanoslot.

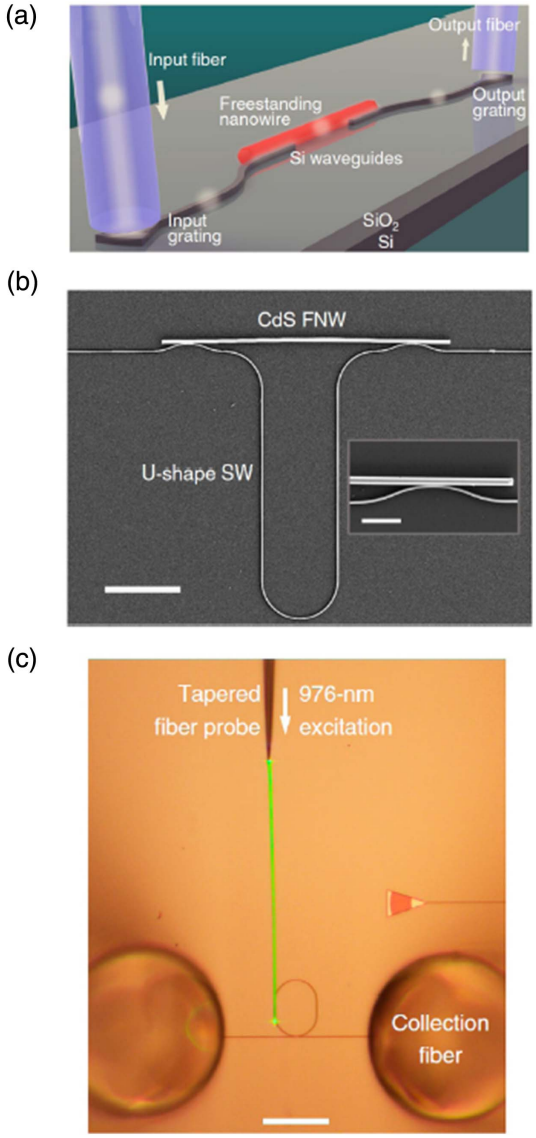

Fig. 3. (a) Schematic of a freestanding nanowire evanescently coupled with integrated silicon waveguide. (b) SEM image of the MZI consisting of a U-shaped 300 nm wide silicon waveguide and a 950 nm diameter CdS free-standing nanowire. The inset shows a close-up view of the right-hand coupling region. (c) Optical micrograph of the integrated nanowire–silicon resonators under a 976 nm wavelength excitation from a tapered fiber probe [70].

For most hybrid approaches described above, silicon waveguides still play an important role in optical confinement, while the cladding materials provide the desired nonlinearity. The commonly used silicon waveguides are single stripe waveguides and nanoslot waveguides. No matter which hybrid structure one chooses, the common principle is to reduce the energy density in silicon to mitigate the detrimental effects of TPA. Another essential problem for efficient nonlinear interactions is the phase-matching condition. The geometric design of the hybrid structure should simultaneously meet the demands of high FOM and phase matching.

C. Utilization of Optical Nanowires with Nonlinearity

Replacing the nonlinear parts of silicon devices with better nonlinear components is also an alternative approach, provided that the coupling efficiency between different components is sufficiently high. In this approach, the introduced structures are separated and have different functions [69]. Very recently, Chen *et al.* demonstrated a hybrid nonlinear free-standing nanowires–silicon waveguide Mach–Zehnder interferometer [Figs. 3(a) and 3(b)] and a racetrack resonator [shown in Fig. 3(c)] for significantly enhanced optical modulation, as well as hybrid active free-standing nanowires–silicon waveguide circuits for light generation [70]. The elaborate near-field coupling structure significantly improved the coupling efficiency between the nanowire and the silicon waveguide to 97% in the telecommunication band, which is much higher than shown in previous works [71,72]. The high efficiency paves the way for a realistic application. Such a hybrid structure has high flexibility and can be extended to diverse nanowires [73,74].

4. LAYERED-MATERIAL-ASSISTED SILICON NONLINEAR PHOTONICS

In recent years, layered material has attracted much attention for its unique and excellent optical and electronic properties. It has great potential for building light sources, modulators, switches, and photon detectors. As a representative, graphene has been studied a lot in the last decade and used for various applications in electro-optic modulation, all-optical modulation, and parametric nonlinear photonics [75], relying on photon absorption and large $\chi^{(3)}$ nonlinearity as well as a unique electronic property. Other layered materials, such as MoS_2, WSe_2, and $MoSe_2$ have $\chi^{(2)}$ nonlinearity on the order of 10^{-7}–10^{-10} m/V, which is comparable to that achievable from commonly used bulk materials. Unlike bulk materials, the integration of ultra-thin layered materials to silicon micro/nano photonics does not require complex fabrication processes. After a direct transfer, the van der Waals force sticks these materials to the silicon surface tightly. More importantly, the layer integration on silicon does not introduce any notable modification of

Table 1. Reported Layered Materials for Nonlinear Silicon Photonics

Material	Type of Nonlinearity ($\chi^{(2)}$, $\chi^{(3)}$, etc.)	Value (SI Unit)	Structure [Waveguide (W), Cavity (C)]	Application
Graphene [76–79]	$\chi^{(3)}$, absorption	$\chi^{(3)} = 3.25 \times 10^{-19}$	W, C	Phase/absorption modulation, bistability
$MoSe_2$ [80]	$\chi^{(2)}$	$\chi^{(2)} = 5 \times 10^{-11}$	W	SHG
MoS_2 [81,82]	$\chi^{(2)}$, $\chi^{(3)}$	$\chi^{(2)} = 10^{-7}$, $\chi^{(3)} = 2.9 \times 10^{-19}$	W, C	SPM, laser
$MoTe_2$ [83]	–	–	C	Laser
WSe_2 [84,85]	$\chi^{(2)}$	$\chi^{(2)} = 6 \times 10^{-11}$	C	SHG, laser

the mode profiles. Furthermore, the silicon waveguide or cavity can also be used to enhance the nonlinear process in these materials. The natural integration compatibility and unique nonlinear property of layered materials encourage the development of hybrid nonlinear silicon photonics. Table 1 refers to the reported layered materials that can be used together with silicon for nonlinear photonics.

A. Utilization of Layered Materials with Parametric Nonlinear Processes

Some layered materials, such as MoS_2 and $MoSe_2$, have a quadratic response to an optical field, so it is possible to combine the material with a silicon waveguide to realize a second-order nonlinear process on silicon. As shown in Fig. 4(a), by covering the $MoSe_2$ layers on top of a silicon waveguide, second harmonic generation from 1550 to 775 nm was observed [80]. The results show a five times enhancement of second harmonic generation compared to the case with only $MoSe_2$ thin layers, demonstrating that the effective nonlinear interaction length is amplified by the silicon waveguide. Note that the harmonic wave of 775 nm was collected from free space. Other materials should be introduced to guide light in the visible region to make an in-plane frequency converter.

Photonic crystal nanocavities are often used to enhance the interaction between the layered materials and optical modes in silicon. Compared with a traditional waveguide, it can provide much stronger nonlinear interaction. It can confine the optical mode to an ultrasmall volume to the order of $(\lambda/n)^3$, where λ is the wavelength and n is the refractive index. The resonant property can also enhance the nonlinear interaction, as well as the small mode volume. In Fig. 4(b), cavity-enhanced second harmonic generation in a WSe_2 covered silicon photonic crystal cavity was realized [84]. The second-order nonlinearity offered by layered materials can pave the way for other nonlinear applications, including low threshold optical parametric oscillation, amplification, and entangled photon pair generation.

In terms of third-order nonlinearity, graphene, black phosphorus, MoS_2, and other layered materials have $\chi^{(3)}$ susceptibility of at least the same order of magnitude with silicon [86,87]. In a silicon photonic crystal cavity covered by graphene, Gu *et al.* observed optical bistability and self-oscillation phenomena [88] [Fig. 4(c)]. In 2015, Liu *et al.* observed an increase in the spectral broadening of the optical pulses in the MoS_2-silicon waveguide compared to the silicon waveguides, indicating the potential application of MoS_2 to enhance the nonlinearity of hybrid silicon photonic devices [81].

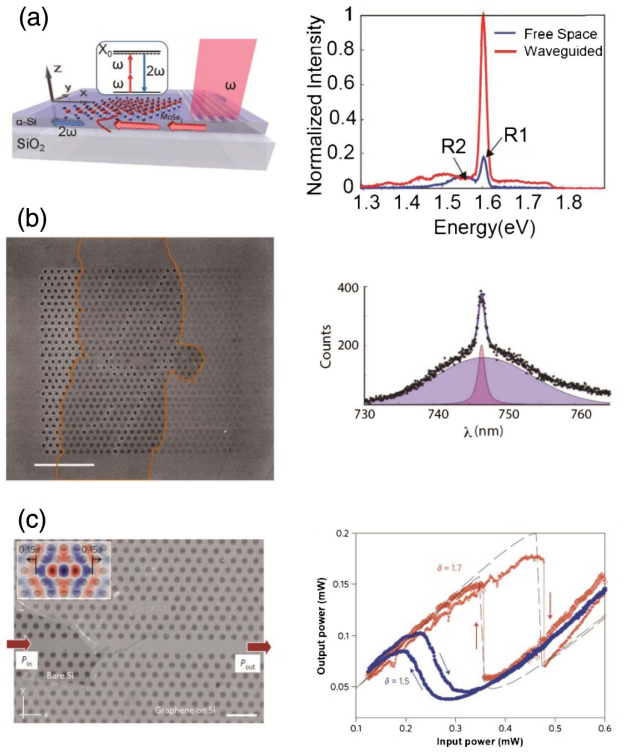

Fig. 4. (a) Schematic design of the hybrid integration of $MoSe_2$ onto a silicon waveguide for second harmonic generation (left). Emission spectrum when excited from grating and free space (right) [80]. (b) Scanning electron micrograph of the fabricated silicon photonic crystal cavity with monolayer WSe_2 on top, indicated by the orange outline. Visible stripes of holes inside the monolayer region are due to the ripped monolayer during exfoliation (left). The spectrum of the second harmonic waves (right) [84]. (c) Scanning electron micrograph of the tuned photonic crystal cavity (left). Steady-state input/output optical bistability for the quasi-TE cavity mode with laser-cavity (right) [88].

B. Utilization of Layered Materials with Light Absorption

TPA and FCA in silicon material have a negative impact on a parametric process, including Kerr, Raman, and Brillouin processes. On the contrary, the nonparametric nonlinear absorption and free carrier effect in silicon can be appropriately controlled to make all-optical modulators. Since the absorption rate and the free carrier induced refractive index change are relevant to the light intensity, the transmission of one mode can be controlled or modified by another light mode [89].

As a zero-band gap material with unique optoelectronic properties, graphene has found applications in photodetectors, solar cells, modulators, and absorbers [90–93]. The electrons in graphene and silicon can exchange with each other, which will influence the electron density in graphene layers and change its optical response. The free carrier effect in a bare silicon waveguide [94] and the optical transmittance of the graphene on top of a silicon waveguide structure [illustrated in Fig. 5(a)] have been elaborately studied by Cheng *et al.*, including the spectral hole burning and saturate absorption [76,77]. By controlling the free carrier density in both materials and their exchange, modulators can be realized by revealing the change of refractive index and absorption. For example, modulators can be realized using the absorption effect, in which the on/off of the control light increases/decreases the loss of waveguide. Another scheme takes advantage of the free carrier induced refractive index change. The modulation is realized using a Mach–Zehnder interferometer to convert the phase modulation to intensity modulation. In 2014, Yu *et al.* realized local and nonlocal optically induced transparency in a graphene-silicon hybrid waveguide using the absorption effect [78]. In this work, the transmission of the signal mode can be controlled all-optically with an optical power as low as 0.1 mW, which is much lower than that needed for a saturable absorption effect. As shown in Fig. 5(b), when the control light is illuminated on the graphene, the photon-generated carriers increase rapidly and flow into the graphene, which changes the transmittance of the signal light. Different from the traditional electric-field induced transparency effect using atoms or cavities, the optically induced transparency is broadband.

The photo-absorptive property of graphene provides the ability to build photon detectors. Because the layer is very thin, the absorption of a few layers of graphene is weak. For a single layer, the absorption is only about 2%. When using a silicon waveguide and cavity, the light absorption in graphene can be enhanced significantly. More than 90% of the light can be absorbed by graphene in a silicon nanocavity, which is promising for detectors with high responsivity. In addition, the absorption and heating of the graphene can increase the nonlinear thermal response of silicon. The thermal nonlinear optical bistability has been observed in a graphene silicon waveguide Fabry–Perot resonator [79].

C. Utilization of Layered Materials with Light Emission

Silicon is an indirect band gap material, so it is hard to integrate a light source on traditional silicon photonics. Even though Raman laser and frequency combs have been demonstrated on a silicon chip, these protocols have a strict requirement of high pump power and high Q cavities. Fortunately, layered materials show great potential to build light sources in atomic scale. It radiates fluorescence under optical excitation and can

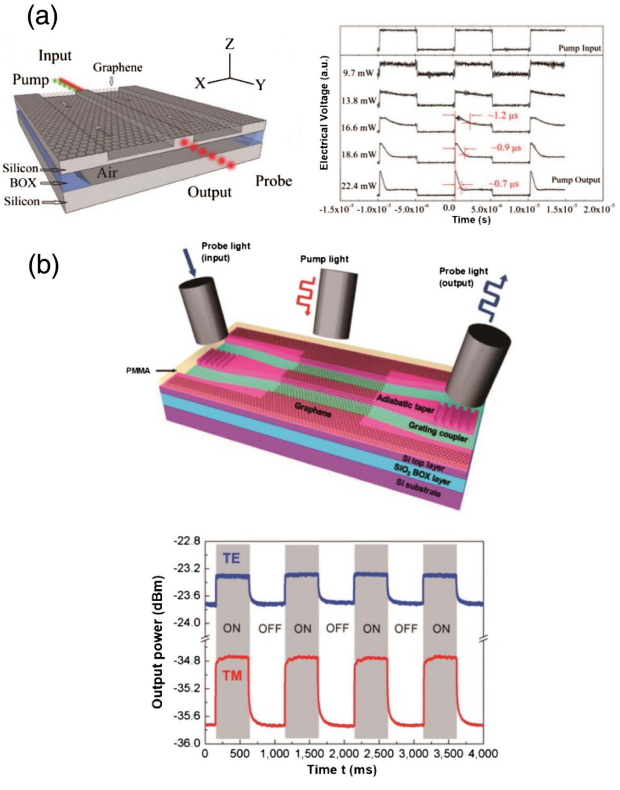

Fig. 5. (a) Schematic picture of an in-plane all-optical modulation in graphene-on-silicon suspended membrane waveguides (left). Pump output power at 100 kHz at different input powers (right) [76,77]. (b) Three-dimensional schematic illustration of a graphene-silicon hybrid nanophotonic wire. The probe light is coupled into and out of the silicon-on-insulator (SOI) nanowire by using grating couplers with adiabatic tapers. The pump light is emitted through a fiber on top of the SOI-nanowire (up). Dynamic responses of the output power for TE- and TM-polarization modes of hybrid nanophotonic wires with a locally modulated optical pump (down) [78].

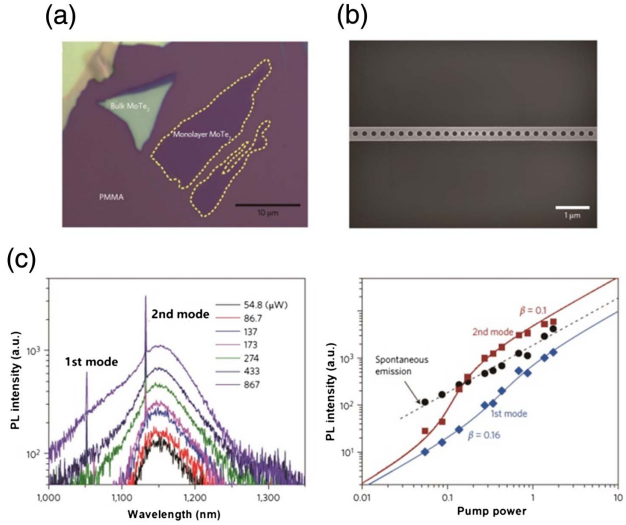

Fig. 6. (a) Optical image of bulk (greenish region) and monolayer $MoTe_2$ (contoured region) on PMMA. (b) Scanning electron micrograph of an undercut silicon nanobeam cavity. The dimensions of the nanobeam cavity are 7.2 μm long, 0.365 μm wide, and 0.22 μm thick. The tightly confined mode in the nanocavity ensures the strong coupling between the layered materials and photons. (c) Left: PL spectra of the nanobeam laser with increasing pump power levels at room temperature, which corresponds to an estimated spectral resolution of 0.41 nm. Right: The log–log plot of light in versus light out for two cavity modes and for a background spontaneous emission shows a clear transition from the spontaneous emission to eventual lasing [83].

find applications in threshold lasers and quantum photon sources [92,93]. Combined with a silicon waveguide or cavity, it is realistic to realize light sources on a silicon chip. At low-temperature, Wu *et al.* observed the lasing behavior of WSe_2 in a photonic crystal cavity [85]. A recent report shows that enhanced and directional emission of monolayer WSe_2 can be controlled by a multiresonant silicon photonic structure [84]. Above the threshold, the silicon cavity-layered material hybrid structure can radiate a laser. In Fig. 6, Ning's group has observed room-temperature continuous-wave lasing from a monolayer $MoTe_2$ integrated with a silicon nanobeam cavity [83]. In addition, some layered materials have defects, which can be treated as an atom. By integrating the layered materials with a silicon waveguide or cavity, the hybrid approach provides a route to build quantum photon sources and study single photon nonlinearity on a silicon chip.

5. SUMMARY

In this review, we have summarized the recent progress in hybrid nonlinear silicon photonics. The hybrid platform takes advantage of silicon and other materials. On one hand, the CMOS-compatible silicon fabrication technology lays the foundation for making high-performance devices. The high optical confinement offered by silicon waveguides and cavities as well as its large nonlinear susceptibility greatly enhances the nonlinear interaction. On the other hand, hybrid structures compensate for the shortcomings of silicon and develop diverse applications. The cladding materials with a second-order nonlinear effect make second harmonic generation and electro-optic modulation possible on a silicon chip. Higher FOM ensures a more efficient and higher data rate wavelength conversion. The integration of silicon with layered materials is naturally compatible and has been demonstrated to realize on-chip room temperature lasing, frequency conversion, all-optical modulation, and photon detection. We believe the combination of silicon and other nonlinear photonic materials can improve the performance and expand the application of on-chip nonlinear silicon photonics.

Funding. National Natural Science Foundation of China (NSFC) (11374263, 61422510, 61431166001, 61725503); Natural Science Foundation of Zhejiang Province (Z18F050002); National Major Research and Development Program (2016YFB0402502).

REFERENCES

1. L. Tsybeskov, D. J. Lockwood, and M. Ichikawa, "Silicon photonics: CMOS going optical [scanning the issue]," Proc. IEEE **97**, 1161–1165 (2009).
2. T. Vallaitis, S. Bogatscher, L. Alloatti, P. Dumon, R. Baets, M. L. Scimeca, I. Biaggio, F. Diederich, C. Koos, W. Freude, and J. Leuthold, "Optical properties of highly nonlinear silicon-organic hybrid (SOH) waveguide geometries," Opt. Express **17**, 17357–17368 (2009).
3. C. K. J. Leuthold and W. Freude, "Nonlinear silicon photonics," Nat. Photonics **4**, 535–544 (2010).
4. M. Lipson, "Guiding, modulating, and emitting light on silicon-challenges and opportunities," J. Lightwave Technol. **23**, 4222–4238 (2005).
5. Y.-H. Kuo, H. Rong, V. Sih, S. Xu, M. Paniccia, and O. Cohen, "Demonstration of wavelength conversion at 40 Gb/s data rate in silicon waveguides," Opt. Express **14**, 11721–11726 (2006).
6. M. A. Foster, R. Salem, D. F. Geraghty, A. C. Turner-Foster, M. Lipson, and A. L. Gaeta, "Silicon-chip-based ultrafast optical oscilloscope," Nature **456**, 81–84 (2008).
7. C. Koos, P. Vorreau, T. Vallaitis, P. Dumon, W. Bogaerts, R. Baets, B. Esembeson, I. Biaggio, T. Michinobu, F. Diederich, W. Freude, and J. Leuthold, "All-optical high-speed signal processing with silicon-organic hybrid slot waveguides," Nat. Photonics **3**, 216–219 (2009).
8. J. T. Robinson, L. Chen, and M. Lipson, "On-chip gas detection in silicon optical microcavities," Opt. Express **16**, 4296–4301 (2008).
9. T. Baehr-Jones, M. Hochberg, G. Wang, R. Lawson, Y. Liao, P. A. Sullivan, L. Dalton, A.-Y. Jen, and A. Scherer, "Optical modulation and detection in slotted silicon waveguides," Opt. Express **13**, 5216–5226 (2005).
10. M. A. Foster, A. C. Turner, R. Salem, M. Lipson, and A. L. Gaeta, "Broad-band continuous-wave parametric wavelength conversion in silicon nanowaveguides," Opt. Express **15**, 12949–12958 (2007).
11. R. Claps, D. Dimitropoulos, V. Raghunathan, Y. Han, and B. Jalali, "Observation of stimulated Raman amplification in silicon waveguides," Opt. Express **11**, 1731–1739 (2003).
12. T. Liang and H. Tsang, "Efficient Raman amplication in silicon-on-insulator waveguides," Appl. Phys. Lett. **85**, 3343–3345 (2004).
13. H. Rong, A. Liu, R. Jones, O. Cohen, D. Hak, R. Nicolaescu, A. Fang, and M. Paniccia, "An all-silicon Raman laser," Nature **433**, 292–294 (2005).
14. M. A. Foster, A. C. Turner, J. E. Sharping, B. S. Schmidt, M. Lipson, and A. L. Gaeta, "Broad-band optical parametric gain on a silicon photonic chip," Nature **441**, 960–963 (2006).
15. E. A. Kittlaus, H. Shin, and P. T. Rakich, "Large Brillouin amplification in silicon," Nat. Photonics **10**, 463–467 (2016).
16. H. K. Tsang, C. Wong, T. Liang, I. Day, S. Roberts, A. Harpin, J. Drake, and M. Asghari, "Optical dispersion, two-photon absorption and self-phase modulation in silicon waveguides at 1.5 μm wavelength," Appl. Phys. Lett. **80**, 416–418 (2002).
17. G. W. Rieger, K. S. Virk, and J. F. Young, "Nonlinear propagation of ultrafast 1.5 μm pulses in high-index-contrast silicon-on-insulator waveguides," Appl. Phys. Lett. **84**, 900–902 (2004).
18. I.-W. Hsieh, X. Chen, X. Liu, J. I. Dadap, N. C. Panoiu, C.-Y. Chou, F. Xia, W. M. Green, Y. A. Vlasov, and R. M. Osgood, "Supercontinuum generation in silicon photonic wires," Opt. Express **15**, 15242–15249 (2007).
19. L. Yin, Q. Lin, and G. P. Agrawal, "Soliton fission and supercontinuum generation in silicon waveguides," Opt. Lett. **32**, 391–393 (2007).
20. T. Baba, "Slow light in photonic crystals," Nat. Photonics **2**, 465–473 (2008).
21. B. Corcoran, C. Monat, C. Grillet, D. J. Moss, B. J. Eggleton, T. White, L. O'Faolain, and T. F. Krauss, "Green light emission in silicon through slow-light enhanced third-harmonic generation in photonic-crystal waveguides," Nat. Photonics **3**, 206–210 (2009).
22. H. Shin, W. Qiu, R. Jarecki, J. A. Cox, R. H. Olsson III, A. Starbuck, Z. Wang, and P. T. Rakich, "Tailorable stimulated Brillouin scattering in nanoscale silicon waveguides," Nat. Commun. **4**, 1944 (2013).
23. W. Qiu, P. T. Rakich, H. Shin, H. Dong, M. Soljacic, and Z. Wang, "Stimulated Brillouin scattering in nanoscale silicon step-index waveguides: a general framework of selection rules and calculating SBS gain," Opt. Express **21**, 31402–31419 (2013).
24. E. A. Kittlaus, N. T. Otterstrom, and P. T. Rakich, "On-chip inter-modal Brillouin scattering," Nat. Commun. **8**, 15819 (2017).
25. R. Dekker, N. Usechak, M. Forst, and A. Driessen, "Ultrafast nonlinear all-optical processes in silicon-on insulator waveguides," J. Phys. D **40**, R249–R271 (2007).
26. R. S. Jacobsen, K. N. Andersen, P. I. Borel, J. Fage-Pedersen, L. H. Frandsen, O. Hansen, M. Kristensen, A. V. Lavrinenko, G. Moulin, H. Ou, C. Peucheret, B. Zsigri, and A. Bjarklev, "Strained silicon as a new electro-optic material," Nature **441**, 199–202 (2006).
27. C. Schriever, F. Bianco, M. Cazzanelli, M. Ghulinyan, C. Eisenschmidt, J. de Boor, A. Schmid, J. Heitmann, L. Pavesi, and J. Schilling, "Second-order optical nonlinearity in silicon waveguides:

inhomogeneous stress and interfaces," Adv. Opt. Mater. **3**, 129–136 (2015).
28. M. Cazzanelli, F. Bianco, E. Borga, G. Pucker, M. Ghulinyan, E. Degoli, E. Luppi, V. Véniard, S. Ossicini, D. Modotto, S. Wabnitz, R. Pierobon, and L. Pavesi, "Second-harmonic generation in silicon waveguides strained by silicon nitride," Nat. Mater. **11**, 148–154 (2011).
29. N. K. Hon, K. K. Tsia, D. R. Solli, and B. Jalali, "Periodically poled silicon," Appl. Phys. Lett. **94**, 091116 (2009).
30. E. Timurdogan, C. V. Poulton, M. J. Byrd, and M. R. Watts, "Electric field-induced second-order nonlinear optical effects in silicon waveguides," Nat. Photonics **11**, 200–206 (2017).
31. R. Jones, H. Rong, A. Liu, A. Fang, M. Paniccia, D. Hak, and O. Cohen, "Net continuous wave optical gain in a low-loss silicon-on-insulator waveguide by stimulated Raman scattering," Opt. Express **13**, 519–525 (2005).
32. H. Rong, S. Xu, Y.-H. Kuo, V. Sih, O. Cohen, O. Raday, and M. Paniccia, "Low-threshold continuous-wave Raman silicon laser," Nat. Photonics **1**, 232–237 (2007).
33. E. Engin, D. Bonneau, C. M. Natarajan, A. S. Clark, M. G. Tanner, R. H. Hadéld, S. N. Dorenbos, V. Zwiller, K. Ohira, N. Suzuki, H. Yoshida, N. Iizuka, M. Ezaki, J. L. O'Brien, and M. G. Thompson, "Photon pair generation in silicon micro-ring resonator with reverse bias enhancement," Opt. Express **21**, 27826–27834 (2013).
34. L. Liao, A. Liu, D. Rubin, J. Basak, Y. Chetrit, H. Nguye, R. Cohen, N. Izhaky, and M. Paniccia, "40 Gbit/s silicon optical modulator for high-speed applications," Electron. Lett. **43**, 1196–1197 (2007).
35. M. P. Nielsen and A. Y. Elezzabi, "Ultrafast all-optical modulation in a silicon nanoplasmonic resonator," Opt. Express **21**, 20274–20279 (2013).
36. T. J. Duffin, M. P. Nielsen, F. Diza, S. Palomba, S. A. Maier, and R. F. Oulton, "Degenerate four-wave mixing in silicon hybrid plasmonic waveguides," Opt. Lett. **41**, 155–158 (2016).
37. I. D. Rukhlenko, M. Premaratne, and G. P. Agrawal, "Nonlinear propagation in silicon-based plasmonic waveguides from the standpoint of applications," Opt. Express **19**, 206–217 (2011).
38. D. Dai and S. He, "A silicon-based hybrid plasmonic waveguide with a metal cap for a nano-scale light confinement," Opt. Express **17**, 16646–16653 (2009).
39. R. Chikkaraddy, B. Nijs, F. Benz, S. J. Barrow, O. A. Scherman, E. Rosta, A. Demetriadou, P. Fox, O. Hess, and J. J. Baumberg, "Single-molecule strong coupling at room temperature in plasmonic nanocavities," Nature **535**, 127–130 (2016).
40. M. A. Foster, K. D. Moll, and A. L. Gaeta, "Optimal waveguide dimensions for nonlinear interactions," Opt. Express **12**, 2880–2887 (2004).
41. M. Jazbinsek, L. Mutter, and P. Gunter, "Photonic applications with the organic nonlinear optical crystal DAST," IEEE J. Sel. Top. Quantum Electron. **14**, 1298–1311 (2008).
42. L. Alloatti, D. Korn, R. Palmer, D. Hillerkuss, J. Li, A. Barklund, R. Dinu, J. Wieland, M. Fournier, J. Fedeli, H. Yu, W. Bogaerts, P. Dumon, R. Baets, C. Koos, W. Freude, and J. Leuthold, "42.7 Gbit/s electro-optic modulator in silicon technology," Opt. Express **19**, 11841–11851 (2011).
43. M. Hochberg, T. Baehr-Jones, G. Wang, J. Huang, P. Sullivan, L. Dalton, and A. Scherer, "Towards a millivolt optical modulator with nano-slot waveguides," Opt. Express **15**, 8401–8410 (2007).
44. T. Baehr-Jones, B. Penkov, J. Huang, P. Sullivan, J. Davies, J. Takayesu, J. Luo, T. D. Kim, L. Dalton, A. Jen, M. Hochberg, and A. Scherer, "Nonlinear polymer-clad silicon slot waveguide modulator with a half wave voltage of 0.25 V," Appl. Phys. Lett. **92**, 163303 (2008).
45. L. Alloatti, D. Korn, C. Weimann, C. Koos, W. Freude, and J. Leuthold, "Second-order nonlinear silicon-organic hybrid waveguides," Opt. Express **20**, 20506–20515 (2012).
46. A. D. Bristow, N. Rotenberg, and H. M. Van Driel, "Two-photon absorption and Kerr coefficients of silicon for 850–2200 nm," Appl. Phys. Lett. **90**, 191104 (2007).
47. T. Wang, N. Venkatram, G. Chen, W. Ji, and D. T. H. Tan, "Optical nonlinearity in silicon at mid-infrared wavelengths," in *Conference on Lasers and Electro-Optics*, OSA Technical Digest (online) (Optical Society of America, 2014), paper STu1I.1.
48. C. Koos, L. Jacome, C. G. Poulton, J. Leuthold, and W. Freude, "Nonlinear silicon-on-insulator waveguides for all-optical signal processing," Opt. Express **15**, 5976–5990 (2007).
49. W. Zhang, S. Serna, N. Dubreuil, and E. Cassan, "Nonlinear optimization of slot Si waveguides: TPA minimization with FOM TPA up to 4.25," Opt. Lett. **40**, 1212–1215 (2015).
50. T. Michinobu, J. C. May, J. H. Lim, C. Boudon, J.-P. Gisselbrecht, P. Seiler, M. Gross, I. Biaggio, and F. Diederich, "A new class of organic donor-acceptor molecules with large third-order optical nonlinearities," Chem. Commun. **6**, 737–739 (2005).
51. J. C. May, I. Biaggio, F. Bures, and F. Diederich, "Extended conjugation and donor-acceptor substitution to improve the third-order optical nonlinearity of small molecules," Appl. Phys. Lett. **90**, 251106 (2007).
52. B. Esembeson, M. L. Scimeca, T. Michinobu, F. Diederich, and I. Biaggio, "A high-optical quality supramolecular assembly for third-order integrated nonlinear optics," Adv. Mater. **20**, 4584–4587 (2008).
53. J. Leuthold, W. Freude, J.-M. Brosi, R. Baets, P. Dumon, I. Biaggio, M. L. Scimeca, F. Diederich, B. Frank, and C. Koos, "Silicon organic hybrid technology: a platform for practical nonlinear optics," Proc. IEEE **97**, 1304–1316 (2009).
54. L. An, H. Liu, Q. Sun, N. Huang, and Z. Wang, "Wavelength conversion in highly nonlinear silicon-organic hybrid slot waveguides," Appl. Opt. **53**, 4886–4893 (2014).
55. T. Vallaitis, C. Heine, R. Bonk, W. Freude, J. Leuthold, C. Koos, B. Esembeson, I. Biaggio, T. Michinobu, F. Diederich, P. Dumon, and R. Baets, "All-optical wavelength conversion at 42.7 Gbit/s in a 4 mm long silicon-organic hybrid waveguide," in *Optical Fiber Communication Conference and National Fiber Optic Engineers Conference*, OSA Technical Digest (CD) (Optical Society of America, 2009), paper OWS3.
56. S. R. Marder, W. E. Torruellas, M. Blanchard-Desce, V. Ricci, G. I. Stegeman, S. Gilmour, J. Bredas, J. Li, G. U. Bublitz, and S. G. Boxer, "Large molecular third-order optical nonlinearities in polarized carotenoids," Science **276**, 1233–1236 (1997).
57. L. Brozozowski and E. H. Sargent, "Azobenzenes for photonic network applications: third-order nonlinear optical properties," J. Mater. Sci. **12**, 483–489 (2001).
58. M. Hochberg, T. Baehr-Jones, G. Wang, M. Shearn, K. Harvard, J. Luo, B. Chen, Z. Shi, R. Lawson, P. Sullivan, A. K. Y. Jen, L. Dalton, and A. Scherer, "Terahertz all-optical modulation in a silicon-polymer hybrid system," Nat. Mater. **5**, 703–709 (2006).
59. B. J. Eggleton, B. Luther-Davies, and K. Richardson, "Chalcogenide photonics," Nat. Photonics **5**, 141–148 (2011).
60. A. Zarifi, A. C. Bedoya, B. Morrison, Y. Zhang, G. Ren, T. Nguyen, S. Madden, K. Vu, A. Mitchell, C. Wolff, D. Marpaung, and B. J. Eggleton, "Nonlinear loss engineering in a silicon-chalcogenide hybrid optical waveguide," in *Nonlinear Photonics* (2016), paper NM4A.6.
61. Z. Yuan, A. Anopchenko, N. Daldosso, R. Guider, D. Navarro-Urrios, A. Pitanti, R. Spano, and L. Pavesi, "Silicon nanocrystals as an enabling material for silicon photonics," Proc. IEEE **97**, 1250–1268 (2009).
62. J. Matres, C. Lacava, G. C. Ballesteros, P. Minzioni, I. Cristiani, J. M. Fédéli, J. Marti, and C. J. Oton, "Low TPA and free-carrier effects in silicon nanocrystal-based horizontal slot waveguides," Opt. Express **20**, 23838–23845 (2012).
63. T. Wu, P. P. Shum, X. Shao, T. Huang, and Y. Sun, "Third harmonic generation from mid-IR to near-IR regions in a phase-matched silicon-silicon-nanocrystal hybrid plasmonic waveguide," Opt. Express **22**, 24367–24377 (2014).
64. I. D. Rukhlenko and V. Kalavally, "Raman amplification in silicon-nanocrystal waveguides," J. Lightwave Technol. **32**, 130–134 (2014).
65. A. Martinez, J. Blasco, P. Sanchis, J. V. Galan, J. García-Rupérez, E. Jordana, P. Gautier, Y. Lebour, S. Hernández, R. Guider, N. Daldosso, B. Garrido, J. M. Fedeli, L. Pavesi, and J. Marti, "Ultrafast all-optical switching in a silicon-nanocrystal-based silicon slot waveguide at telecom wavelengths," Nano Lett. **10**, 1506–1511 (2010).
66. Z. Kang, J. Yuan, X. Zhang, Q. Wu, X. Sang, G. Farrell, C. Yu, F. Li, H. Y. Tam, and P. K. A. Wai, "CMOS-compatible 2-bit optical spectral quantization scheme using a silicon-nanocrystal-based horizontal slot waveguide," Sci. Rep. **4**, 7177 (2014).

67. Q. Liu, S. Gao, Z. Li, Y. Xie, and S. He, "Dispersion engineering of a silicon-nanocrystal-based slot waveguide for broadband wavelength conversion," Appl. Opt. **50**, 1260–1265 (2011).
68. V. M. N. Passaro, F. De Leonardis, and A. G. Perri, "Investigation of dispersion and nonlinear effects in silicon nanocrystal slot waveguides for surface optical sensing," IEEE Sens. J. **12**, 2776–2783 (2012).
69. H. Kim, A. C. Farrell, P. Senanayake, W.-J. Lee, and D. L. Huffaker, "Monolithically integrated InGaAs nanowires on 3D structured silicon-on-insulator as a new platform for full optical links," Nano Lett. **16**, 1833–1839 (2016).
70. B. Chen, H. Wu, C. Xin, D. Dai, and L. Tong, "Flexible integration of free-standing nanowires into silicon photonics," Nat. Commun. **8**, 20 (2017).
71. H.-G. Park, C. J. Barrelet, Y. Wu, B. Tian, F. Qian, and C. M. Lieber, "A wavelength-selective photonic-crystal waveguide coupled to a nanowire light source," Nat. Photonics **2**, 622–626 (2008).
72. P. L. Nichols, Z. Liu, L. Yin, S. Turkdogan, F. Fan, and C.-Z. Ning, "$Cd_xPb_{1-x}S$ alloy nanowires and heterostructures with simultaneous emission in mid-infrared and visible wavelengths," Nano Lett. **15**, 909–916 (2015).
73. Y. Nakayama, P. J. Pauzauskie, A. Radenovic, R. M. Onorato, R. J. Saykally, J. Liphardt, and P. Yang, "Tunable nanowire nonlinear optical probe," Nature **447**, 1098–1101 (2007).
74. R. Yan, D. Gargas, and P. Yang, "Nanowire photonics," Nat. Photonics **3**, 569–576 (2009).
75. S. Yu, X. Wu, Y. Wang, X. Guo, and L. Tong, "2D materials for optical modulation: challenges and opportunities," Adv. Mater. **29**, 14 (2017).
76. Z. Cheng, H. K. Tsang, K. Xu, and Z. Shi, "Spectral hole burning in silicon waveguides with a graphene layer on top," Opt. Lett. **38**, 1930–1932 (2013).
77. Z. Cheng, H. K. Tsang, X. Wang, K. Xu, and J. B. Xu, "In-plane optical absorption and free carrier absorption in graphene-on-silicon waveguides," IEEE J. Sel. Top. Quantum Electron. **20**, 43–48 (2014).
78. L. Yu, J. Zheng, Y. Xu, D. Dai, and S. He, "Local and nonlocal optically induced transparency effects in graphene-silicon hybrid nanophotonic integrated circuits," ACS Nano **8**, 11386–11393 (2014).
79. C. Horvath, D. Bachman, R. Indoe, and V. Van, "Photo-thermal nonlinearity and optical bistability in a graphene-silicon waveguide resonator," Opt. Lett. **38**, 5036–5039 (2013).
80. H. Chen, V. Corboliou, A. S. Solntsev, D.-Y. Choi, D. de Ceglia, C. de Angelis, Y. Lu, and D. N. Neshev, "Enhanced second-harmonic generation from two-dimensional $MoSe_2$ by waveguide integration," Light Sci. Appl. **6**, e17060 (2017).
81. L. Liu, K. Xu, X. Wan, J. Xu, C. Y. Wong, and H. K. Tsang, "Enhanced optical Kerr nonlinearity of MoS_2 on silicon waveguides," Photon. Res. **3**, 206–209 (2015).
82. O. Salehzadeh, M. Djavid, N. H. Tran, I. Shih, and Z. Mi, "Optically pumped two-dimensional MoS_2 lasers operating at room-temperature," Nano Lett. **15**, 5302–5306 (2015).
83. Y. Li, J. Zhang, D. Huang, H. Sun, F. Fan, J. Feng, Z. Wang, and C. Z. Ning, "Room-temperature continuous-wave lasing from monolayer molybdenum ditelluride integrated with a silicon nanobeam cavity," Nat. Nanotechnol. **12**, 987–992 (2017).
84. T. K. Fryett, K. L. Seyler, J. Zheng, C.-H. Liu, and X. Xu, "Silicon photonic crystal cavity enhanced second harmonic generation from monolayer WSe_2," arXiv: 1607.03548 (2016).
85. S. Wu, S. Buckley, J. R. Schaibley, L. Feng, J. Yan, D. G. Mandrus, F. Hatami, W. Yao, J. Vuckovic, A. Majumdar, and X. Xu, "Monolayer semiconductor nanocavity lasers with ultralow thresholds," Nature **520**, 69–72 (2015).
86. J. B. Khurgin, "Graphene–a rather ordinary nonlinear optical material," Appl. Phys. Lett. **104**, 161116 (2014).
87. T. Fryett, A. Zhan, and A. Majumdar, "Cavity nonlinear optics with layered materials," arXiv: 1708.05099 (2017).
88. T. Gu, N. Petrone, J. F. McMillan, A. van der Zande, M. Yu, G. Q. Lo, D. L. Kwong, J. Hone, and C. W. Wong, "Regenerative oscillation and four-wave mixing in graphene optoelectronics," Nat. Photonics **6**, 554–559 (2012).
89. D. J. Moss, L. Fu, I. Littler, and B. Eggleton, "Ultrafast all-optical modulation via two-photon absorption in silicon-on-insulator waveguides," Electron. Lett. **41**, 320–321 (2005).
90. L. Liao, Y.-C. Lin, M. Bao, R. Cheng, J. Bai, Y. Liu, Y. Qu, K. L. Wang, Y. Huang, and X. Duan, "High speed graphene transistors with a self-aligned nanowire gate," Nature **467**, 305–308 (2010).
91. M. Liu, X. Yin, E. Ulin-Avila, B. Geng, T. Zentgraf, L. Ju, F. Wang, and X. Zhang, "A graphene-based broadband optical modulator," Nature **474**, 64–67 (2011).
92. Z. Sun, A. Martinez, and F. Wang, "Optical modulators with 2D layered materials," Nat. Photonics **10**, 227–238 (2016).
93. F. Xia, T. Mueller, Y.-M. Lin, A. Valdes-Garcia, and P. Avouris, "Ultrafast graphene photodetector," Nat. Nanotechnol. **4**, 839–843 (2009).
94. Y. Liu and H. K. Tsang, "Time dependent density of free carriers generated by two photon absorption in silicon waveguides," Appl. Phys. Lett. **90**, 211105 (2007).